The Astrophysical Journal, 711:1062–1072, 2010 March 10 doi:10.1088/0004-637X/711/2/1062

MULTIPLE PLASMOID EJECTIONS AND ASSOCIATED HARD X-RAY BURSTS IN THE 2000 NOVEMBER 24 FLARE

N. Nishizuka[1], H. Takasaki[1,2], A. Asai[3,4], and K. Shibata[1]
[1] Kwasan and Hida Observatories, Kyoto University, Yamashina, Kyoto 607-8471, Japan; nisizuka@kwasan.kyoto-u.ac.jp
[2] Accenture Japan, Ltd., Akasaka Inter City, Akasaka, Minato-ku, Tokyo 107-8672, Japan
[3] Nobeyama Solar Radio Observatory, National Astronomical Observatory of Japan, Minamisaku, Nagano 384-1305, Japan
[4] The Graduate University for Advanced Studies (SOKENDAI), Miura, Kanagawa 240-0193, Japan
Received 2009 July 17; accepted 2010 January 27; published 2010 February 22

ABSTRACT

The Soft X-ray Telescope (SXT) on board *Yohkoh* revealed that the ejection of X-ray emitting plasmoid is sometimes observed in a solar flare. It was found that the ejected plasmoid is strongly accelerated during a peak in the hard X-ray (HXR) emission of the flare. In this paper, we present an examination of the *GOES* X 2.3 class flare that occurred at 14:51 UT on 2000 November 24. In the SXT images, we found "multiple" plasmoid ejections with velocities in the range of 250–1500 km s^{-1}, which showed blob-like or loop-like structures. Furthermore, we also found that each plasmoid ejection is associated with an impulsive burst of HXR emission. Although some correlation between plasmoid ejection and HXR emission has been discussed previously, our observation shows similar behavior for multiple plasmoid ejection such that each plasmoid ejection occurs during the strong energy release of the solar flare. As a result of temperature-emission measure analysis of such plasmoids, it was revealed that the apparent velocities and kinetic energies of the plasmoid ejections show a correlation with the peak intensities in the HXR emissions.

Key words: acceleration of particles – instabilities – magnetohydrodynamics (MHD) – Sun: coronal mass ejections (CMEs) – Sun: flares – X-rays: bursts

Online-only material: animations, color figures

1. INTRODUCTION

The Soft X-ray Telescope (SXT; Tsuneta et al. 1991) on board *Yohkoh* (Ogawara et al. 1991) revealed that a soft X-ray emitting plasma ejection, or plasmoid ejection, is sometimes observed in solar flares (e.g., Shibata et al. 1995). It was also found that the plasmoids show blob-like or loop-like shapes and that the strong acceleration of the plasmoid ejection occurs during the peak time of the hard X-ray (HXR) emission (Tsuneta 1997; Ohyama & Shibata 1997). Their ejection velocities are typically several hundred km s^{-1} and the ejected plasma is heated to more than 10 MK before the onset of the ejection (Ohyama & Shibata 1997, 1998). They often start to rise up gradually a few tens of minutes before the onset of a HXR burst and are then strongly accelerated just before or at the impulsive phase of the flare. A similar kinetic evolution is also seen in the case of coronal mass ejections (CMEs; Zhang et al. 2001; Kim et al. 2005a, 2005b).

Similarly, slowly drifting radio structures, observed at the beginning of the eruptive solar flares in the 0.6–1.5 GHz frequency range, have been interpreted as the radio signatures of plasmoid ejection (Kliem et al. 2000; Khan et al. 2002; Karlický et al. 2002). Hudson et al. (2001), moreover, identified a rapidly moving HXR source associated with a moving microwave source and an X-ray plasmoid ejection. Kundu et al. (2001) also identified moving soft X-ray ejecta associated with moving decimetric/metric radio sources observed by the Nançay radioheliograph. Sui et al. (2004) also found a plasmoid ejection in HXR images with the *RHESSI* satellite.

In the standard model of solar flares, the so-called CSHKP model (Carmichael 1964; Sturrock 1966; Hirayama 1974; Kopp & Pneuman 1976), a filament/plasmoid ejection is included. However, it does not necessarily explicitly stress the importance of the role of plasmoid ejection . Shibata et al. (1995) and Shibata & Tanuma (2001) extended the CSHKP model by unifying reconnection and plasmoid ejection and stressed the importance of the plasmoid ejection in a reconnection process. The model is called the "plasmoid-induced-reconnection" model. In that model, the plasmoid inhibits reconnection and stores magnetic energy in a current sheet. Then, once it is ejected, inflow is induced because of the mass conservation, resulting in the enhancement of reconnection rate and the acceleration of the plasmoid due to the faster reconnection outflow. Moreover, reconnection theories predict several plasmoids of various scales are generated. The dynamics of plasmoid formation in the solar flare and their subsequent plasmoid ejection affect the reconnection rate in the nonlinear evolution. Therefore, plasmoid ejections are observational evidence of magnetic reconnection of solar flares. Since plasmoid ejections have been observed in both long duration events and compact flares (Shibata et al. 1995), it is shown that the magnetic reconnection model may be applicable even for the compact flares that do not show the other typical features of the magnetic reconnection.

On the basis of the results of magnetohydrodynamic (MHD) numerical simulations, Kliem et al. (2000) suggested that each individual burst in the slowly pulsating structure is generated by suprathermal electrons, accelerated in the peak of the electric field in the quasi-periodic and bursting regime of the magnetic field reconnection. This is the so-called impulsive bursty reconnection (Priest 1985). In that regime, several plasmoids can be formed successively as a result of the tearing and coalescence instabilities (Finn & Kaw 1977; Kliem et al. 2000). The repeated formation of magnetic islands can induce magnetic reconnection and their subsequent coalescence (Tajima et al. 1987). These processes even have a cascading form: secondary tearing, tertiary tearing, and so on, always on smaller and smaller spatial scales (Tanuma et al. 2001; Shibata & Tanuma 2001). Furthermore, the formed plasmoids can merge into larger plasmoids. Tanuma et al. (2001) also showed that an increase in the velocity

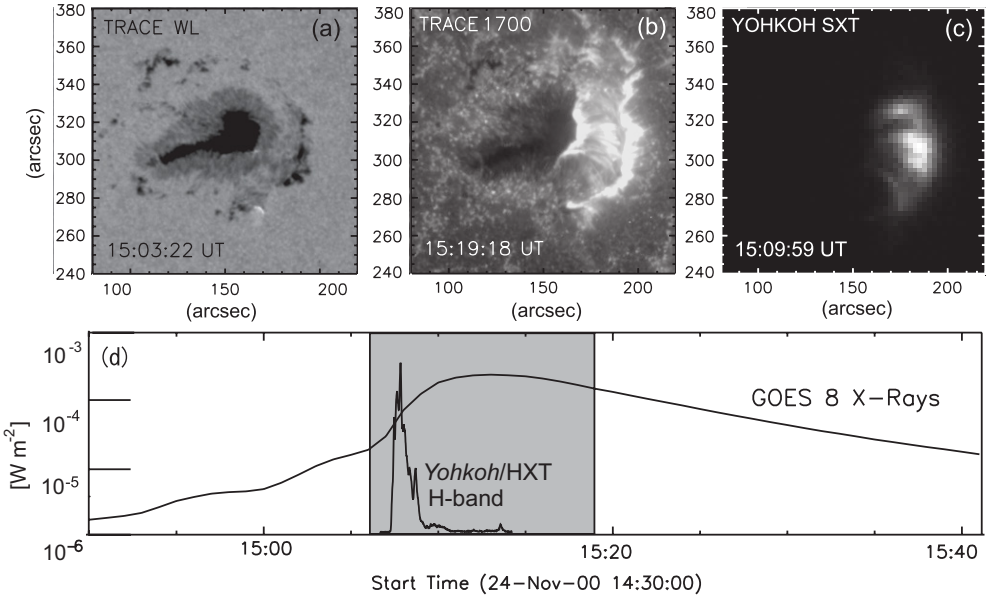

Figure 1. (a) Snapshot image of the preceding sunspot of NOAA Active Region 9236 taken with the white light filter of the *Transition Region and Coronal Explorer* (*TRACE*; Handy et al. 1999; Schrijver et al. 1999). (b) Snapshot image of the two-ribbon flare and the coronal loops located at the west side of the sunspot taken with the 1700 Å filter of *TRACE* and (c) full-resolution image of *Yohkoh*/SXT. (d) *GOES* soft X-ray flux and the HXR emission observed with *Yohkoh*/HXT.

of the plasmoid ejection leads to an increase in the reconnection rate, and Bárta et al. (2008) analyzed the dynamics of plasmoids formed by the current sheet tearing.

The unsteady reconnection mentioned above can release a large amount of energy in a quasi-periodic way. The energy released in the upward direction can be observed as plasmoid ejections or CMEs, while that in the downward direction as downflows (McKenzie & Hudson 1999; Asai et al. 2004b) and impulsive bursts at the footpoints of the coronal loops. Bursty energy release in solar flares has been observed as highly time variable HXR bursts and microwave bursts (Frost & Dennis 1971; Dennis 1985; Kane & Anderson 1970; Kiplinger et al. 1983; Benz & Aschwanden 1992; Aschwanden 2002). Benz & Aschwanden (1992) and Aschwanden (2002) argued that these impulsive bursts suggest the existence of highly fragmented particle acceleration regions. This fragmented structure of solar flares indicates that a flare is an ensemble of a vast amount of small-scale energy releases and the fractal/turbulent structure of the current sheet can be expected (see also Nishizuka et al. 2009). Recently the kinematics of multiple plasmoids have been studied by full-particle simulations and how the particles interact with their surroundings has been explained (e.g., Drake et al. 2006; Pritchett 2008; Drake et al. 2009; Daughton et al. 2009). It is interesting to note that the stochastic acceleration mechanism (e.g., Benz & Smith 1987; Brown & Loran 1985; Miller et al. 1996; Liu et al. 2006) may be related to particle acceleration in fractal/turbulent current sheet (see also Strauss 1988; Kowal et al. 2009; Samtaney et al. 2009).

Karlický et al. (2004) showed a unique series of slowly drifting structures during one flare, from which the authors proposed that it indirectly maps a formation of several plasmoids and their interactions. However in most of the previous studies, only one plasmoid or one drifting structure was reported during the solar flare. In this paper, we present for the first time the direct observations of multiple X-ray emitting plasmoid ejections associated with a single solar flare observed by *Yohkoh*/SXT (firstly reported by Takasaki 2006). In Section 2, we describe the multiple plasmoid ejection events. Then we analyzed the data in Section 3 by examining in detail the relationship between the multiple plasmoid ejections and the nonthermal HXR emissions using *Yohkoh* data. Finally, we discuss the dynamic features of magnetic reconnection and the role of plasmoid ejections in the particle acceleration in a solar flare in Section 4.

2. OBSERVATION

2.1. Overview

A series of homologous flare-CME events occurred in NOAA Active Region 9236 from 2000 November 24 to November 26. These events have been reported by several researchers. Nitta & Hudson (2001) found that the CME-flare events of the homologous flares show quite similar characteristics in both their coronal/photospheric magnetic structures and their CME properties. Zhang & Wang (2002) compared the homologous flares in detail through the use of multiwavelength observations. Wang et al. (2002) reported that the activities of these flares were driven or triggered by newly emerging magnetic flux, which appeared on the western side of the leading sunspot in this active region. Figures 1(a)–(c) show snapshot images of the preceding sunspot in NOAA 9236 and an associated two-ribbon flare, which occurred on 2000 November 24 observed in white light, ultraviolet, and soft X-ray emission. Takasaki et al. (2004) performed a comparison of the physical parameters between the individual flares and from this they could confirm that the plasmoid-induced-reconnection model is reasonable. They then showed that the interaction between the new emerging magnetic flux loops and the pre-existing magnetic field was essential for producing the homologous flares and plasmoid ejections in the active region.

These ejections were followed by a single halo-CME which occurred at 15:30 UT on 2000 November 24. Figure 2 shows a CME image observed with the Large Angle Spectroscopic Coronagraph (LASCO; Brueckner et al. 1995) that occurred following the flare (e.g., see Nitta & Hudson 2001; Zhang & Wang 2002). The core of the CME was observed traveling in the northwest direction. Moon et al. (2003) found a good

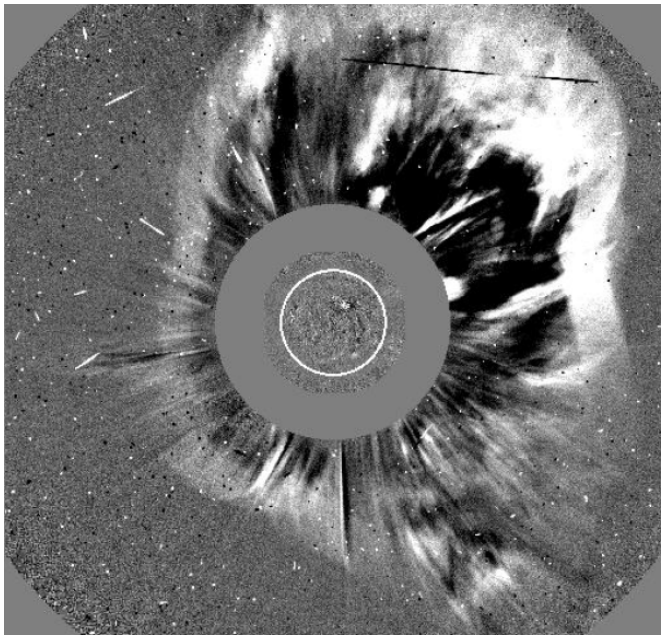

Figure 2. Running difference image of the CME taken with C2 LASCO on board *Solar and Heliospheric Observatory* (Domingo et al. 1995) at 16:00 UT on 2000 November 24.

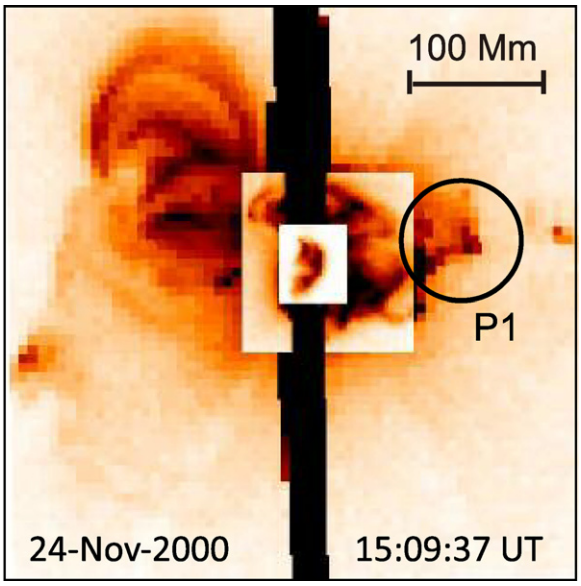

Figure 3. Time evolution of the flare which occurred at 14:51 UT on 2000 November 24. This is made of full-, half-, and quarter-resolution images taken with *Yohkoh*/SXT AlMg filter (negative images). (Movie 1; courtesy of J. Kiyohara)

(An animation and color version of this figure is available in the online journal.)

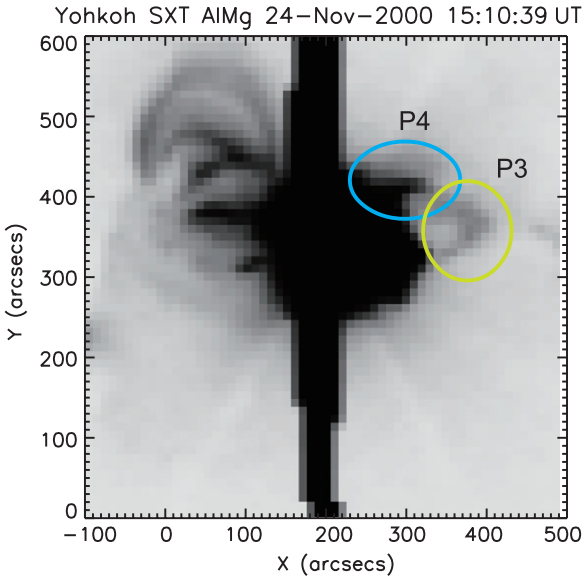

Figure 4. Multiple plasmoid ejections associated with the flare on 2000 November 24, which are marked with color circles (movie 2). This is made of quarter-resolution images taken with *Yohkoh*/SXT AlMg filter (negative images).

(An animation and color version of this figure is available in the online journal.)

correlation between CME speed and the *GOES* X-ray peak flux of the associated flares in this series of homologous flare-CME events.

Impulsive HXR bursts were also observed in this flare with the Hard X-ray Telescope (HXT; Kosugi et al. 1991) on board *Yohkoh* (see Figure 1(d)). A pair of HXR sources was located at the footpoints of the coronal arcade. We used the HXR emission data observed with the *H* band (52.7–92.8 keV) of HXT, whose temporal resolution was 0.5 s.

2.2. Multiple Plasmoid Ejections

We focus on a *GOES* X2.3 class flare that occurred in NOAA 9236 (N19°, W06°) at 14:51 UT on 2000 November 24. This flare was one of the homologous flares which were described previously. In this flare, we observed seven plasmoid ejections in the soft X-ray images of the flare taken with *Yohkoh*/SXT. We mainly used the partial frame images with half- and quarter-resolution for the analysis. The spatial resolutions are about 5″ and 10″, respectively. We used the sandwich (AlMg) filter images which were taken with 20 s cadence. Figure 3 and supplement movie 1 show the temporal evolution of the flare, which is made of full-, half-, and quarter-resolution images taken with *Yohkoh*/SXT AlMg filter (negative images). Full-, half-, and quarter-resolution images are different in their spatial resolutions, field of views, and exposure times. Full-resolution images are of short exposure time and focus on the brightest region of the active region, such as the two ribbon structure. On the other hand, quarter-resolution images are of longer exposure time so that they are applicable for the detection of large-scale and faint phenomena such as plasmoid ejections. The black vertical line in the middle of Figure 3 shows the saturation of the quarter-resolution images. We identified seven major ejections which we named P1–P7. In Figures 4 (movie 2) through 6, we marked each plasmoid ejection with a circle. Each plasmoid ejection can be seen more clearly in quarter-resolution images of Figure 5, while half-resolution images of Figure 6 are convenient to see plasmoids just after ejections. The fields of view of quarter- and half-resolution images are also shown in Figure 3.

Figure 7 shows the temporal evolution of soft X-ray emission observed with SXT. A full resolution image is inset into Figure 7(a). Figures 7(a)–(c) shows three of the plasmoid ejections denoted as P1, P4, and P7. In Figures 7(d)–(f), we overlaid contour images of the soft X-ray emission, which show the time evolution of the plasmoid ejection. The directions of the ejections are indicated by the arrows in the panels. To make clear the traveling of the plasmoids, we also overlaid

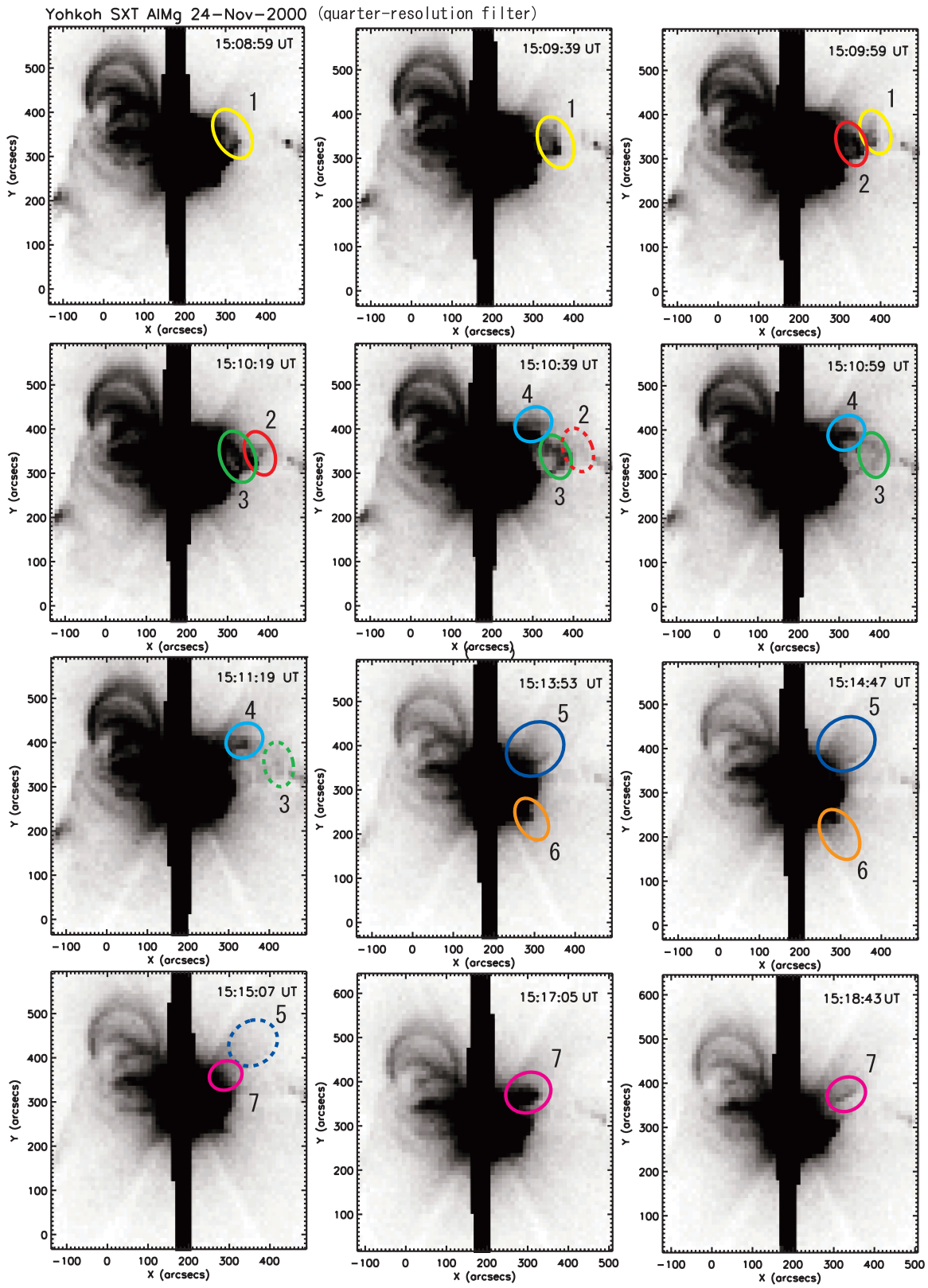

Figure 5. Series of snapshot images of multiple plasmoid ejections associated with a flare on 2000 November 24. They are quarter-resolution images of the sandwich (AlMg) filters of SXT on board *Yohkoh*. Each plasmoid ejection is marked with a circle and indices of ejection number.

(A color version of this figure is available in the online journal.)

the contours of the SXR images taken at different times (e.g., 15:09:19 UT, 15:09:39 UT and 15:09:59 UT for Figure 7(d)) on Figures 7(d)–(f). From these contour images, we can roughly outline the position and the size of the bright cores of the plasmoids. We can also measure the velocity V by taking the time difference of these contour images. Those size and apparent

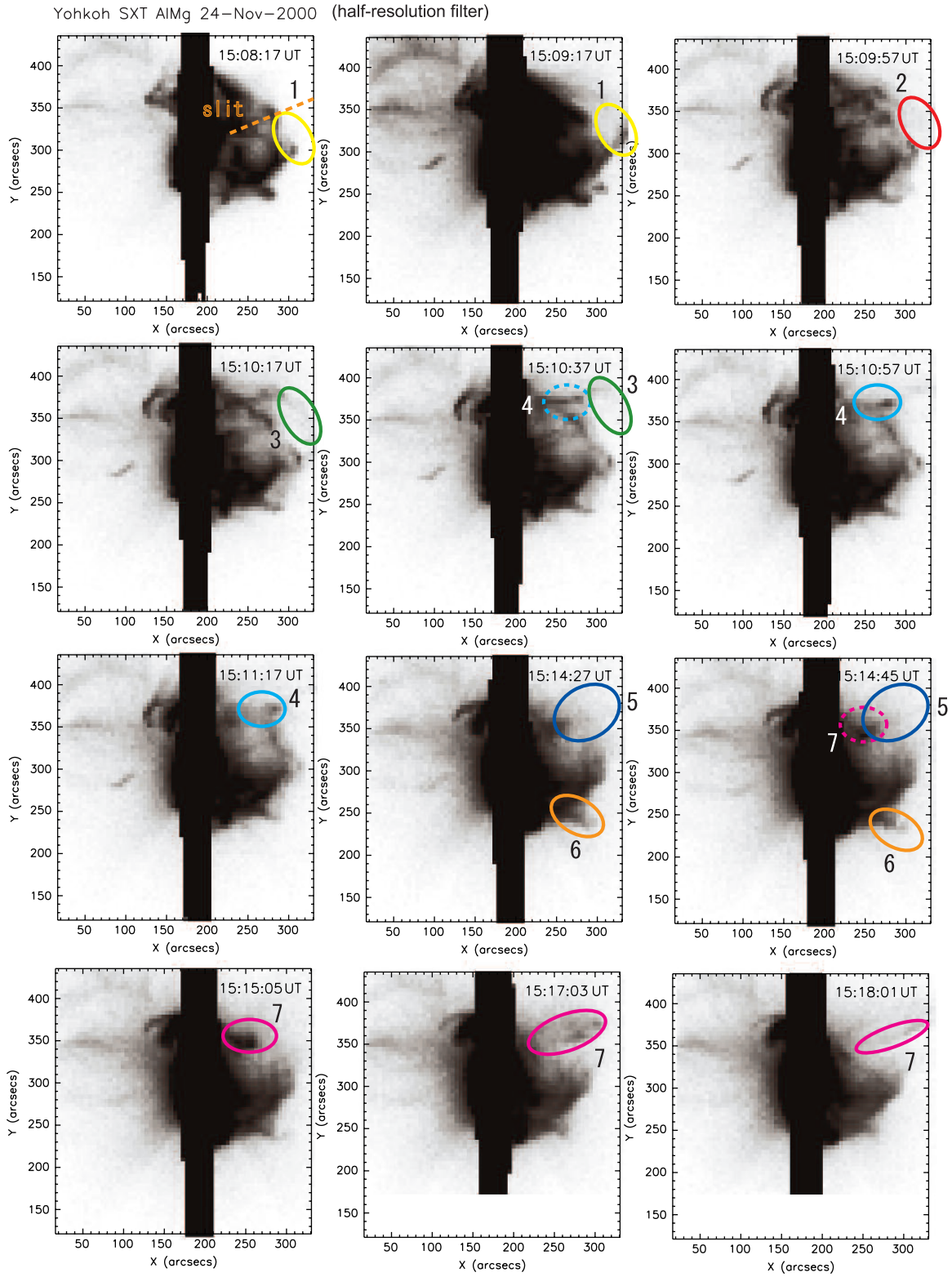

Figure 6. Series of snapshot images of multiple plasmoid ejections associated with a flare on 2000 November 24. They are half-resolution images of the sandwich (AlMg) filters of SXT on board *Yohkoh*. Each plasmoid ejection is marked with a circle and indices of ejection number. Dotted line shows the slit position, along which the time slice image of Figure 8 was made.

(A color version of this figure is available in the online journal.)

velocity of the plasmoids are listed in Table 1. Here we note that these are the "apparent" velocities, and the motions in the line of sight are ignored. Therefore, the actual velocity of the plasmoid $V/\cos\theta$ will be greater than the plane-of-the-sky value, where $1/\cos\theta$ represents the expected deprojection over a reasonable range of angles θ to the plane of the sky. The trajectory of the plasmoid is not necessarily in the straight lines as shown with the arrows in Figure 7. In order to take into account those

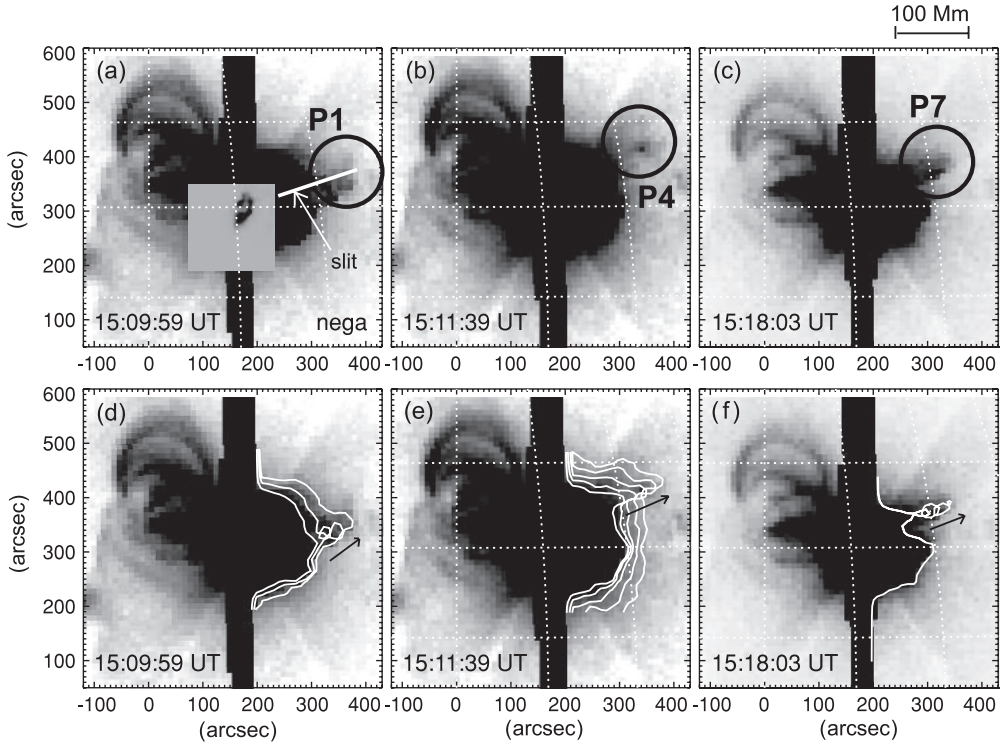

Figure 7. Snapshot images of three different plasmoid ejections occurred at 15:00 UT on 2000 November 24 taken with *Yohkoh*/SXT AlMg filter (negative images). (a)–(c) Quarter-resolution images and a full-resolution image of SXT. Plasmoid ejections are denoted with the number of P1, P4, and P7. A full-resolution image in (a) shows the same two-ribbon structure as shown in Figure 1. (d)–(f) The time evolution of the plasmoid ejections. Contour plots of the plasmoids of (d) are taken at 15:09:19 UT, 15:09:39 UT, and 15:09:59 UT, while (e) at 15:10:39 UT, 15:10:59 UT, 15:11:19 UT, 15:11:39 UT, and 15:11:59 UT, and (f) at 15:16:45 UT, 15:17:23 UT, and 15:18:03 UT.

non-straight motions, we measured the apparent velocity of each plasmoid by averaging the velocities derived from each time differences. In the following discussions, we consider the apparent velocity as the actual velocity.

We can see several plasmoids were ejected in the northwest direction, and one plasmoid ejected in the southwest direction in Figures 4 (movie 2) and 5, which is marked as P6 in this paper. Each plasmoid has a unique velocity, brightness, and size. The first ejection was that of P1, which was followed by P2–P4 which were successively ejected as a group in the same direction. P1 shows blob-like structure, while P2–P4 seem to be a part of an expanding loop. We are not able to clearly define the structure of P5 and P6 due to the faint emission, although we can surely identify P5 and P6 traveling outward from the active region. P7 is the brightest ejection of blob-like structure. It starts to rise up gradually at 15:12 UT and ejected/accelerated upward at 15:14 UT.

In the LASCO CME images, we can no longer identify the fine structure corresponding to the individual plasmoid ejections, though some complicated structures can be observed (see Figure 2). This is probably because the ejected plasmoids merge into a single CME. The average velocity of the CME listed in the CME event catalog[5] is about 1245 km s^{-1}. This apparent velocity of the CME is faster than those of the plasmoid ejections P1–P7 summarized in Table 1. This observational fact qualitatively suggests that the merged plasmoids are continuously accelerated as they are ejected into interplanetary space, as shown by Cheng et al. (2003), although we can hardly identify the one-to-one relation between them.

[5] CME event catalog: http://cdaw.gsfc.nasa.gov/CME_list/.

3. ANALYSIS AND RESULTS

3.1. Time Slice Images of Plasmoid Ejections and Comparison to the Hard X-ray Bursts

Here we focus on the time evolution of the plasmoid ejections. We used a time slice image of the plasmoid ejections as we show in Figure 8. The horizontal axis is the time from 15:06 UT to 15:18 UT, and the vertical axis is the one-dimensional image (negative images) using a slit line placed along the direction of the several plasmoid ejections (P1, P3, P4, P5, and P7). This time slice image is made of half-resolution images. The position of the slit line is shown in Figures 6 and 7(a). Those ejections seen in the time slice image are marked with signs □, △, . . . in Figure 8(b). We can also identify further additional faint ejections in the time slice image. Some ejections travel along the slit lines, while others travel on a path which is slightly different from the slit line. As a result, the visibility of each plasmoid ejection is different.

Initially P1, P2, and P3 are slowly accelerated, then strongly accelerated during the initial impulsive phase of the hard X-ray emission (15:07:40–15:08:40 UT) followed closely by the ejection of P4. A group of plasmoids gradually rise up 15:09:40–15:12:20 UT followed by the faint ejection P5. P6 is ejected in a different direction (southwest) and does not cross the slit line, so it does not appear in Figures 8(a) and (b). P7 is the brightest ejection and the most clearly visible in Figures 8(a) and (b). The apparent velocities of the plasmoids along the slit can also be derived from the slopes of the fitted lines in Figure 8(b). We note that these are the apparent velocities measured from the time slice images of Figure 8(b) and different from the velocities measured from contour plot images in Figure 7. This

Table 1
Physical Parameters of the Multiple Plasmoid Ejections

Plasmoid Ejections	Time (UT)	log T (K)	log EM (cm^{-3})	Size (10^{18} cm^2)	Density (10^9 cm^{-3})	Mass (10^{13} g)	Velocity (km s^{-1})	E_{kin} (10^{28} erg)	E_{th} (10^{28} erg)	Direction	I_{HXR} (CTS s^{-1} sc^{-1})
P1	15:09:19–15:09:59	6.98–7.09	45.32–45.33	>3.9–4.7	2.76–2.79	>2.63–2.66	654–818	>5.63–8.91	>2.51–3.28	Northwest	1000
P2	15:09:59–15:10:59	(7.00)	(45.34)	>4.6–5.8	(2.65)	>(3.69)	573–654	(>6.05–7.88)	(>3.69)	Northwest	1300
P3	15:10:19–15:10:59	(7.00)	(45.32)	>4.7–8.3	(2.59)	>(3.60)	982–1470	(>17.4–38.9)	(>3.60)	Northwest	1500
P4	15:10:39–15:11:19	7.02–7.07	45.80–45.80	>3.1–7.1	4.85	>4.30	654–828	>9.19–14.7	>4.50–5.05	Northwest	950
P5	15:13:33–15:14:27	7.02–7.08	45.73–45.74	>1.5–3.1	5.76–5.83	>1.12–1.13	360–844	>0.72–4.03	>1.17–1.36	Northwest	120
P6	15:13:33–15:13:51	7.07–7.11	45.49–45.50	>1.6–5.2	4.37–4.42	>0.85–0.86	360–720	>0.55–2.22	>0.99–1.11	Southwest	130
P7	15:16:27–15:18:43	6.97–7.03	46.05–46.06	>3.2–7.8	6.95–7.03	>3.99–4.04	254–409	>1.29–3.38	>3.72–4.33	Northwest	150
Total	...	...	...	...	...	...	...	43.5–84.7	20.2–22.4		
Flare	15:18:33–15:18:53	6.73–7.08	48.27–48.96	9.33	137–304	391–865	...	...	210–1040		

Notes. We assumed that the line-of-sight width of a plasmoid is equal to the square-root of the size. As for plasmoid ejections P2 and P3, there are no Be/thick Al filter images so that we assumed temperature of the plasmoids as 10^7 K. We used two images of the thick Al filter just before and after the one of the Be filter. The error in Table 1 comes from the result of these two images. This error is much greater than that of photon noise (see Ohyama & Shibata 1997 in more detail).

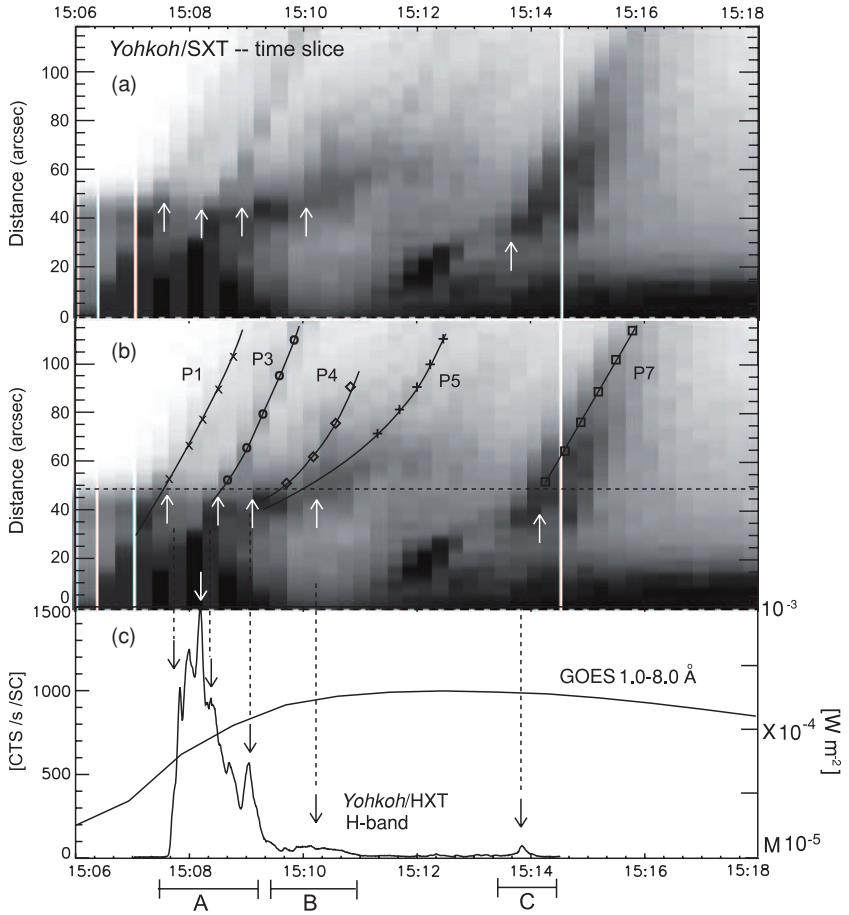

Figure 8. (a) Apparent height of the plasmoids ejected in the 2000 November 24 flare at 15:00 UT. Time slice image is obtained with half-resolution images of *Yohkoh*/SXT. The signs of plus (+), circle (○), triangle (△) and square (□) are plotted over the time slice image in (b). (c) Counting rates of HXR emission observed with the *H* band (52.7–92.8 keV channel) of *Yohkoh*/HXT and the corresponding *GOES* soft X-ray light curve.

is because the former shows the front velocity of thinner density plasma, while the latter shows the velocity of the thick core part of the plasmoids. In Figures 8(a) and (b), the plasmoid ejections roughly start to rise at the apparent height of approximately 50″ (∼35 Mm) and propagate into the upper atmosphere. This probably means that reconnection occurs at around or just below the height of ∼35 Mm. In this paper, we set the start position of plasmoid ejections as the height (∼35 Mm) and define the start times of ejections as the time when each plasmoid crosses the height (which is shown with dotted line in Figure 8(b)). It is noted that Figures 6 and 8(a) and (b) are drawn with half-resolution images, but Figure 5 is a series of quarter-resolution images. Therefore, we see more of the earlier phase of plasmoid ejection in Figures 6 and 8 than in Figure 5, and so Figure 8 is more appropriate to determine the time of plasmoid ejection. We confirmed that the start times are comparable to those defined above.

In Figure 8(c), we show the light curve of the HXR emission obtained with the *H* band (52.7–92.8 keV) of *Yohkoh*/HXT and the *GOES* soft X-ray light curve. We can distinguish the HXR bursts into three separate periods: the first period, A (15:08–15:09 UT), is the brightest phase of the HXR emission, the second period, B (15:09–15:11 UT), show gradual enhancement, and the last period, C (∼15:14 UT), is an isolated HXR peak. The plasmoid ejections of P1–P3 seem to be ejected during the peak time of period A. P1 seems to be ejected just before the HXR peaks in Figure 8(c). This is consistent with the report by Ohyama & Shibata (1997) who showed that plasmoids are ejected at or just before the HXR peak. During period B, a group of plasmoids gradually rise up and are followed by the faint ejection of P4 and P5, while the brightest plasmoid P7 is ejected during period C. The correspondence of the plasmoid ejections and HXR peaks is shown by the arrows in Figure 8(b). Since the bursts in period A are superposed and very complex, it is difficult to identify the exact correspondence between the plasmoid ejections (P1–P3) and the hard X-ray bursts.

We made a correlation plot of the times of the HXR bursts and those of the plasmoid ejections (Figure 9(a)) to make the relation clearer. Both the horizontal and vertical axes show the times (UT). The horizontal (light gray) and the vertical (dark gray) lines illustrate the times of the plasmoid ejections and those of the HXR bursts, respectively. The thickness of the lines shows an estimation of the error. Figure 9(b) shows HXR (52.7–92.8 keV) light curves obtained with *H* band of *Yohkoh*/HXT. The thin solid line shows the points where the times of the plasmoid ejections correspond to those of the HXR bursts. These results appear to show that several plasmoid ejections coincide with HXR bursts.

Here we note that although the intense HXR emissions indicate that strong energy releases occur at those times, it does not necessarily mean that certain amount of plasmoids, that is, notable plasmoids are ejected. We have already noticed that there are many fainter ejections, which also tend to appear at HXR bursts, while some of the hard X-ray intensity fluctuations

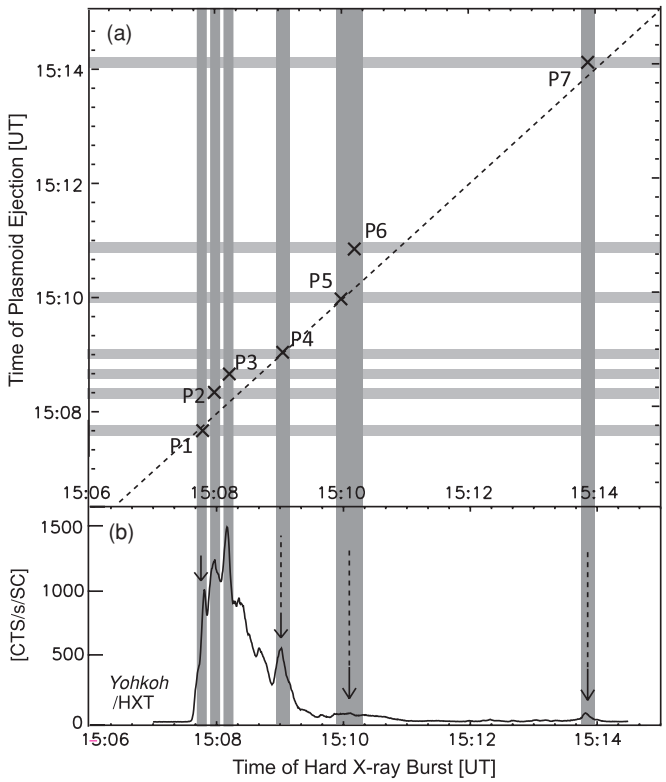

Figure 9. (a) Correlation plot between the times of the hard X-ray (HXR) bursts and those of the plasmoid ejections. Both the horizontal and vertical axes show the times (UT). The horizontal (light gray) and the vertical (dark gray) thick lines illustrate the times of the plasmoid ejections and those of the HXR bursts, respectively. The width of the thick lines shows the amount of error approximately. (b) HXR (52.7–92.8 keV) light curves obtained with *H* band of *Yohkoh*/HXT. The thin solid line shows the points where the times of the plasmoid ejections correspond to those of the HXR bursts.

have no associated ejections in Figures 8 and 9. On the other hand, the HXR burst for P5 and P6 does not show a sharp summit but a gentle hump. This is probably because ejections P5 and P6 are parts of continuous outflows from the active region during this time range. This may also suggest a milder energy release compared with the others, resulting into a gradual enhancement of HXR emission between 15:09:40 UT and 15:11:00 UT.

3.2. Temperature Diagnostics of Seven Plasmoid Ejections

We also studied temperature diagnostics on the soft X-ray emitting plasma using the SXT filter ratio method (Hara et al. 1992). We used the half-resolution images taken with the Be and thick Al filters of SXT for the analysis of plasmoid ejections. We subtracted the background photon flux of plasmoids. The temperature and emission measure are determined using the two filter data of the Be and thick Al filters. The size of the plasmoid S was measured from the contour plot images in Figure 7(b), which shows the lower limit of the observable size (summarized in Table 1). We assume that the X-ray emitting plasma, measured by the filter ratio method, fills the plasmoid with a filling factor of 1. We assumed that the volume of the plasmoid is $S^{3/2}$, such that the line-of-sight width of a plasmoid is equal to the square-root of the size S. Since the observation times of the Be and thick Al filters are not exactly the same, we used two images from the thick Al filter which were taken just before and just after the Be filter observation. The error shown in Table 1 mostly results from combining these two images. This error is much greater than the background photon noise (see Ohyama & Shibata 1997, in more detail). As for plasmoid ejections P2 and P3, there are no Be and thick Al filter images, because P2 and P3 are out of field of view of half-resolution images as shown in Figure 6. In these cases, we assumed the temperatures of P2 and P3 as 10^7 K.

Table 1 summarizes the physical parameters, such as temperature, emission measure, density, mass, thermal energy, and kinetic energy of each plasmoid, of the seven plasmoid ejections identified in Figure 5. Since the size of the plasmoids that we derived from the images is just the lower limit, the mass, thermal and kinetic energies calculated with the size are also the lower limit. In Table 1, each plasmoid shows a typical temperature of 10^7 K, a density of 10^9 cm^{-3}, and an apparent velocity of 200–1400 km s^{-1}, which is similar to results of previous studies (i.e., Ohyama & Shibata 1997, 1998). The kinetic energy of each plasmoid ejection seems to be comparable to or twice as large as their thermal energy. We also estimate the total flare energy from the full-resolution images (spatial resolution 2.″5) of the same filters at the peak time of *GOES* soft X-ray emission. Since the only part of the total flare energy is converted into plasmoid ejections, the total energy of plasmoid ejections is smaller than the total energy of solar flare.

4. SUMMARY AND DISCUSSION

We analyzed the *GOES* X2.3 class flare which occurred at 14:51 UT on 2000 November 24. We found multiple plasmoid ejections from a single flare. Furthermore, each plasmoid ejection seems to be associated with a peak in the HXR emission.

In Figure 8, the plasmoid ejections seem to occur at the height of approximately 50″ (∼35 Mm). This tells us that reconnection occurs at the height of approximately 35 Mm. The horizontal light gray lines in the top panel of Figure 9 show that the times of plasmoid ejections, when they reach the height of 35 Mm, seems to be well correlated to the peak time of HXR emission, which is consistent with previous studies (e.g., Ohyama & Shibata 1997). Since the peak in HXR emission indicates strong energy release, we have demonstrated that each plasmoid ejection occurs during a period of strong energy release, suggesting a series of impulsive energy releases in a single flare.

We also performed a temperature and emission measure analysis and investigated the physical parameters of the plasmoid ejections shown in Table 1. Figure 8 and Table 1 show that the HXR bursts in period A have large intensities in correlation with the large kinetic energy of plasmoid ejections P1–P4. Conversely, the HXR bursts in periods B and C have small intensities in correlation with the kinetic energy of plasmoid ejections P5–P7. Figure 10(a) shows the relation between the kinetic energy of plasmoid ejection and the intensity of the corresponding HXR peak emission. We can see a rough tendency that the larger kinetic energy of plasmoid ejections is associated with the brighter HXR peak emission, and vice versa. The HXR emission is known to show energy release rate (e.g., Neupert effect; Neupert 1968; Asai et al. 2004a), which leads us to the following equation:

$$I_{\rm HXR}\Delta t \sim \frac{dI_{\rm SXR}}{dt}\Delta t \propto \frac{dE_{\rm th}}{dt}\Delta t \sim \Delta E_{\rm th} \sim \Delta E_{\rm kin} \sim \frac{1}{2}mV_{\rm pl}^2, \quad (1)$$

where we assumed that the released thermal energy of a solar flare in a short period is comparable to the kinetic energy of the plasmoid ejection. This means that a plasmoid ejection with large HXR emission, and therefore with large energy release,

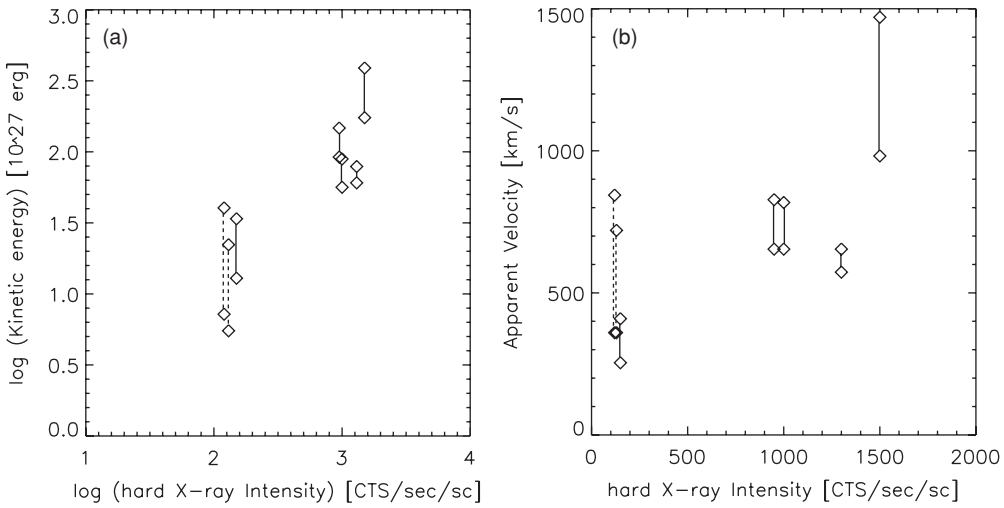

Figure 10. (a) Correlation plot between the kinetic energy of plasmoid ejection and the intensity of the corresponding hard X-ray peak emission. (b) Correlation plot between the apparent velocity of plasmoid ejection and the intensity of the corresponding HXR peak emission.

can be accelerated strongly. A similar kinetic evolution is also seen in the case of CMEs (Yashiro & Gopalswamy 2009).

Figure 10(b) shows the relation between the apparent velocity and the intensity of the corresponding HXR peak emissions. There seems to be a correlation between the plasmoid velocities and the HXR emissions, although it is difficult to measure the velocities of the plasmoids precisely due to the faint emission. Similar to the above equations, we can derive the following relation between HXR emission and the kinetic energy of a plasmoid ejection:

$$I_{\rm HXR} \sim \frac{dI_{\rm SXR}}{dt} \propto \frac{dE_{\rm th}}{dt} \sim \frac{B^2}{4\pi} v_{\rm in} L^2 \propto V_{\rm CME} \sim V_{\rm pl}. \quad (2)$$

Here B is the typical magnetic field in a current sheet, $v_{\rm in}$ is the inflow velocity and L is the characteristic length of the inflow region. The inflow velocity $v_{\rm in}$ is thought to be about $0.01 v_A$ from direct observations (Yokoyama et al. 2001; Narukage & Shibata 2006). It has been also known that inflow can be controlled by the plasmoid ejection. As a plasmoid is ejected out of the current sheet, the density in the current sheet decreases, and the inflow is enhanced to conserve the total mass under the condition that incompressibility is approximately satisfied. Here, we assume that $v_{\rm in}$ is proportional to the plasmoid velocity $V_{\rm pl}$. Then, we find the relation $I_{\rm HXR} \propto V_{\rm pl}$. Moreover, if we can further assume the $V_{\rm pl}$ is proportional to CME velocity $V_{\rm CME}$, then $I_{\rm HXR} \propto V_{\rm CME}$. This is consistent with the result of Yashiro & Gopalswamy (2009). A correlation between the energy release rate, which is represented by $I_{\rm HXR}$, and the plasmoid velocity $V_{\rm pl}$ is also successfully reproduced by a MHD simulation (Nishida et al. 2009). In the simulation, they clearly showed that the plasmoid velocity controls the energy release rate (i.e., reconnection rate) in the nonlinear evolution.

Observations of plasmoid ejections have been paid attention to as evidence of magnetic reconnection, though only one plasmoid ejection per solar flare has been found. However, magnetic reconnection theory suggests that the impulsive bursty regime of reconnection or fractal reconnection is associated with a series of plasmoids of various scales. It is known that magnetic reconnection is an effective mechanism for energy release in a solar flare. Once the current sheet becomes thin enough for the tearing instability to occur, repetitive formation of magnetic islands and their subsequent coalescence drives the "impulsive bursty" regime of reconnection (Finn & Kaw 1977; Tajima et al. 1987; Priest 1985). Furthermore, such reconnection can produce a fractal structure in the current sheet, which is not only theoretically predicted but has also been observed (i.e., Shibata & Tanuma 2001; Nishizuka et al. 2009). The plasmoids generated in this cycle control the energy release by inhibiting magnetic reconnection in the current sheet and/or by inflow driven by the ejection. The plasmoid ejection enhances reconnection and promotes further plasmoid ejections from the current sheet. Similar intermittent energy release from a solar flare has been reported as multiple downflows associated with HXR bursts in the impulsive phase (Asai et al. 2004b). McKenzie & Savage (2009) estimated the total amount of energy of multiple downflows and showed that it is comparable to the total amount of energy released from the magnetic field, which is consistent with the magnetic reconnection model. Tanuma et al. (2001) showed through numerical simulations that plasmoid ejections are closely coupled with the reconnection process and the greatest energy release occurs when the largest plasmoid is ejected. If the strong energy release corresponds to magnetic reconnection, we may conclude that this is evidence of unsteady magnetic reconnection in a solar flare and that plasmoids have a key role in energy release and particle acceleration.

We first acknowledge an anonymous referee for his/her useful comments and suggestions. We also thank A. Hillier for his careful reading and correction of this paper. We also thank J. Kiyohara for her help in making the movies and T. Morimoto for his help in finding the multiple plasmoid ejection events. We made extensive use of *Yohkoh*/SXT and HXT data. This work was supported in part by the Grant-in-Aid for Creative Scientific Research "The Basic Study of Space Weather Prediction" (Head Investigator: K. Shibata) from the Ministry of Education, Culture, Sports, Science, and Technology of Japan, and in part by the Grand-in-Aid for the Global COE program "The Next Generation of Physics, Spun from Universality and Emergence" from the Ministry of Education, Culture, Sports, Science, and Technology (MEXT) of Japan.

REFERENCES

Asai, A., Yokoyama, T., Shimojo, M., Masuda, S., Kurokawa, H., & Shibata, K. 2004a, ApJ, 611, 557

Asai, A., Yokoyama, T., Shimojo, M., & Shibata, K. 2004b, ApJ, 605, L77
Aschwanden, M. J. 2002, Particle Acceleration and Kinematics in Solar Flares (Dordrecht: Kluwer)
Bárta, M., Vršnak, B., & Karlický, M. 2008, A&A, 477, 649
Benz, A. O., & Aschwanden, M. J. 1992, in Lecture Notes in Physics 399, Eruptive Solar Flares, ed. Z. Svestka, B. V. Jackson, & M. E. Machado (New York: Springer), 106
Benz, A. O., & Smith, D. F. 1987, Sol. Phys., 107, 299
Brueckner, G. E., et al. 1995, Sol. Phys., 162, 357
Brown, J. C., & Loran, J. M. 1985, MNRAS, 212, 245
Carmichael, H. 1964, in The Physics of Solar Flares, ed. W. N. Hess (NASA SP-50; Washington, DC: NASA), 451
Cheng, C. Z., Ren, Y., Choe, G. S., & Moon, Y. -J. 2003, ApJ, 596, 1341
Daughton, W., Roytershteyn, V., Albright, B. J., Karimabadi, H., Yin, L., & Bowers, K. J. 2009, Phys. Rev. Lett., 103, 065004
Dennis, B. R. 1985, Sol. Phys., 100, 465
Domingo, V., Fleck, B., & Poland, A. I. 1995, Sol. Phys., 162, 1
Drake, J. F., Cassak, P. A., Shay, M. A., Swisdak, M., & Quataert, E. 2009, ApJ, 700, L16
Drake, J. F., Swisdak, M., Che, H., & Shay, M. A. 2006, Nature, 433, 553
Finn, J. M., & Kaw, P. K. 1977, Phys. Fluids, 20, 72
Frost, K. J., & Dennis, B. R. 1971, ApJ, 165, 655
Handy, B. N., et al. 1999, Sol. Phys., 187, 229
Hara, H., Tsuneta, S., Lemen, J. R., Acton, L. W., & McTiernan, J. M. 1992, PASJ, 44, L135
Hirayama, T. 1974, Sol. Phys., 34, 323
Hudson, H. S., Kosugi, T., Nitta, N. V., & Shimojo, M. 2001, ApJ, 561, L211
Kane, S. R., & Anderson, K. A. 1970, ApJ, 162, 1003
Karlický, M., Fárník, F., & Mészárosová, H. 2002, A&A, 395, 677
Karlický, M., Fárník, F., & Kurucker, S. 2004, A&A, 419, 365
Khan, J. I., Vilmer, N., Saint-Hilaire, P., & Benz, A. O. 2002, A&A, 388, 363
Kim, Y.-H., Moon, Y.-J., Cho, K.-S., Bong, S.-C., & Park, Y. D. 2005a, ApJ, 635, 1291
Kim, Y.-H., Moon, Y.-J., Cho, K.-S., Kim, K.-S., & Park, Y. D. 2005b, ApJ, 622, 1240
Kiplinger, A. L., Dennis, B. R., Emslie, A. G., Frost, K. J., & Orwig, L. E. 1983, ApJ, 265, L99
Kliem, B., Karlický, M., & Benz, A. O. 2000, A&A, 360, 715
Kopp, R. A., & Pneuman, G. W. 1976, Sol. Phys., 50, 85
Kosugi, T., et al. 1991, Sol. Phys., 136, 17
Kowal, G., Lazarian, A., Vishniac, E. T., & Otmianowska-Mazur, K. 2009, ApJ, 700, 63
Kundu, M. R., Nindos, A., Vilmer, N., Klein, K.-L., Shibata, K., & Ohyama, M. 2001, ApJ, 559, 443
Liu, S., Petrosian, V., & Mason, G. M. 2006, ApJ, 636, 462
McKenzie, D. E., & Hudson, H. S. 1999, ApJ, 519, L93
McKenzie, D. E., & Savage, S. L. 2009, ApJ, 697, 1569
Miller, J. A., LaRosa, T. N., & Moore, R. L. 1996, ApJ, 461, 445
Moon, Y.-J., Choe, G. S., Wang, H., Park, Y. D., & Cheng, C. Z. 2003, Korean Astron. Soc., 36, 61
Narukage, N., & Shibata, K. 2006, ApJ, 637, 1122
Neupert, W. M. 1968, ApJ, 153, L59
Nitta, N. V., & Hudson, H. S. 2001, Geophys. Res. Lett., 28, 3801
Nishida, K., Shimizu, M., Shiota, D., Takasaki, H., Magara, T., & Shibata, K. 2009, ApJ, 690, 748
Nishizuka, N., Asai, A., Takasaki, H., Kurokawa, H., & Shibata, K. 2009, ApJ, 694, L74
Ogawara, Y., Takano, T., Kato, T., Kosugi, T., Tsuneta, S., Watanabe, T., Kondo, I., & Uchida, Y. 1991, Sol. Phys., 136, 1
Ohyama, M., & Shibata, K. 1997, PASJ, 49, 249
Ohyama, M., & Shibata, K. 1998, ApJ, 499, 934
Priest, E. R. 1985, Rep. Prog. Phys., 48, 955
Pritchett, P. L. 2008, Phys. Plasma, 15, 102105
Samtaney, R., Loureiro, N. F., Uzdensky, D. A., Schekochihin, A. A., & Cowley, S. C. 2009, Phys. Rev. Lett., 103, 105004
Schrijver, C. J., et al. 1999, Sol. Phys., 187, 261
Shibata, K., Masuda, S., Shimojo, M., Hara, H., Yokoyama, T., Tsuneta, S., Kosugi, T., & Ogawara, Y. 1995, ApJ, 451, L83
Shibata, K., & Tanuma, S. 2001, Earth Planets Space, 53, 473
Strauss, H. R. 1988, ApJ, 326, 412
Sturrock, P. A. 1966, Nature, 211, 695
Sui, L., Holman, G. D., & Dennis, B. R. 2004, ApJ, 612, 546
Tajima, T., Sakai, J., Nakajima, H., Kosugi, T., Brunel, F., & Kundu, M. R. 1987, ApJ, 321, 1031
Takasaki, H. 2006, PhD thesis, Kyoto Univ.
Takasaki, H., Asai, A., Kiyohara, J., Shimojo, M., Terasawa, T., Takei, Y., & Shibata, K. 2004, ApJ, 613, 592
Tanuma, S., Yokoyama, T., Kudoh, T., & Shibata, K. 2001, ApJ, 551, 312
Tsuneta, S. 1997, ApJ, 483, 507
Tsuneta, S., et al. 1991, Sol. Phys., 136, 37
Wang, H., Gallagher, P., Yurchyshyn, V., Yang, G., & Goode, P. R. 2002, ApJ, 569, 1026
Yashiro, S., & Gopalswamy, N. 2009, in Proc IAU Symp. 257, Universal Heliophysical Processes, ed. N. Gopalswamy & D. F. Webb (Cambridge: Cambridge Univ. Press), 233
Yokoyama, T., Akita, K., Morimoto, T., Inoue, K., & Newmark, J. 2001, ApJ, 546, L69
Zhang, J., Dere, K. P., Howard, R. A., Kundu, M. R., & White, S. M. 2001, ApJ, 559, 452
Zhang, J., & Wang, J. 2002, ApJ, 566, L117